Hurricane boundary layer observation and modeling challenges

Jun Zhang

NOAA/AOML/Hurricane Research Division & University of Miami

The 2nd Boundary Layer Workshop, 1 June 2021

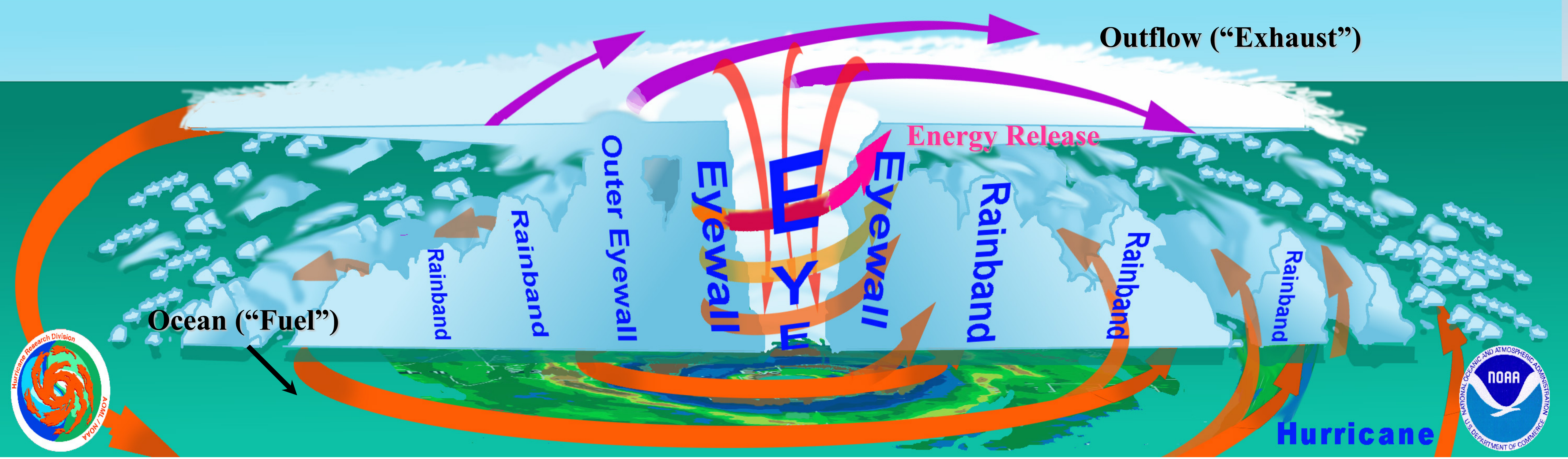

$$|V_{\max}|^2 \approx \frac{C_k}{C_D}\frac{T_s - T_0}{T_0}(k_0^* - k)$$

Emanuel (1986,1995)

$C_K/C_D > 0.75$

V_{max} - maximum intensity

k- enthalpy

T_s - SST

T_0 - outflow temperature

C_D - drag coefficient (momentum)

C_K - enthalpy exchange coefficient

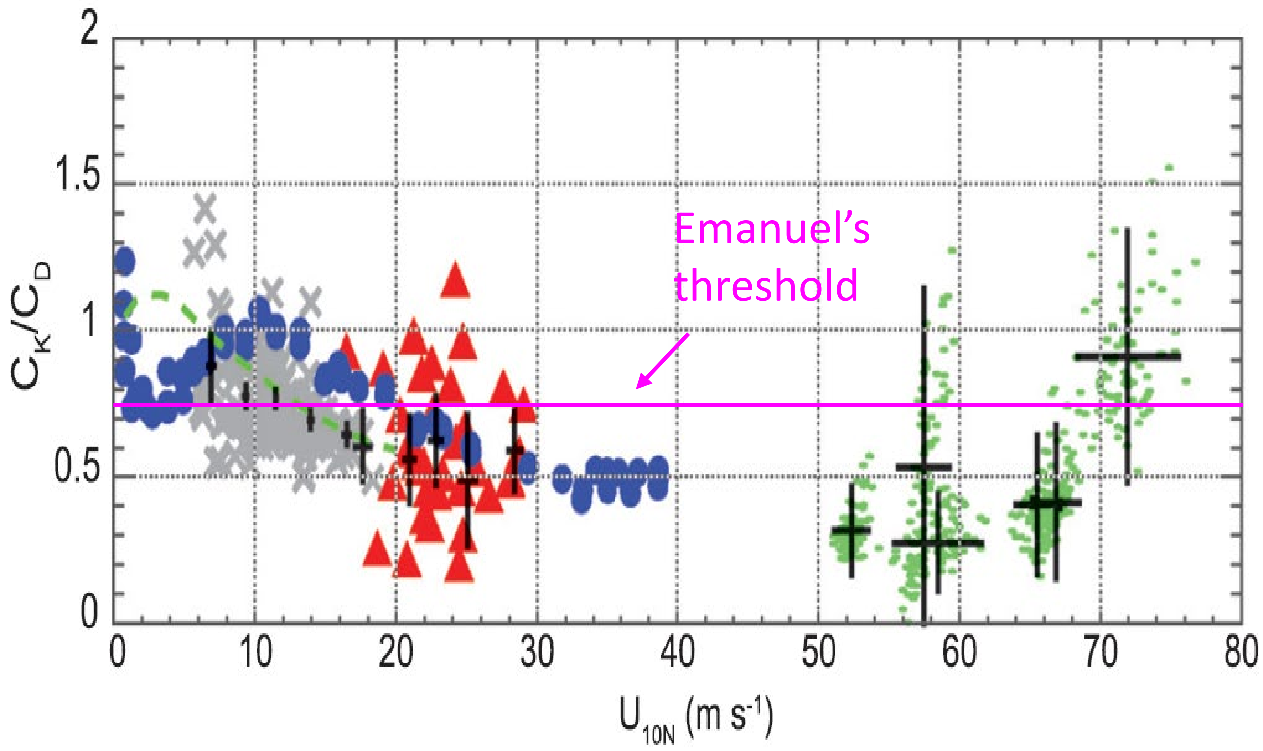

Gray crosses - HEXOS – Eddy Correlation (EC) method (DeCosmo et al. 1996)
Red triangles - CBLAST - EC method (Zhang et al. 2008)
Blue circles - Wave tank exp - budget (Haus et al. 2010)
Green dots – observation-based budget (Bell et al. 2012)

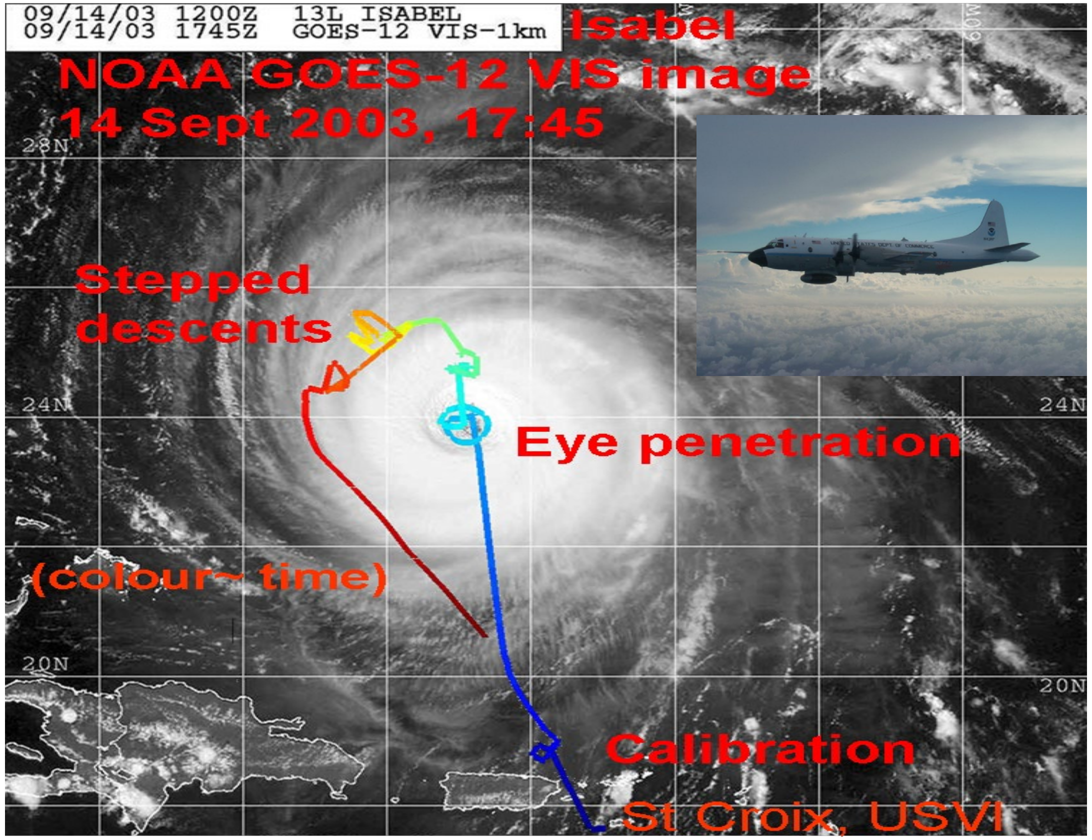

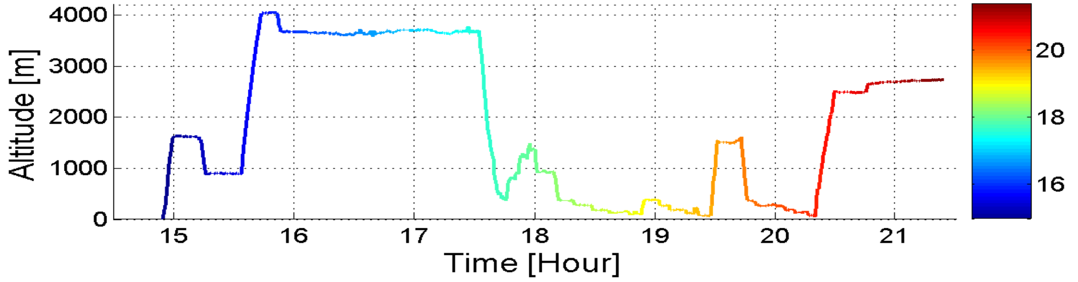

- Observational studies (e.g, Zhang et al. 2008; Bell et al. 2012) found that C_K/C_D can be statistically significantly smaller than 0.75 for surface wind speed of 20-70 m/s, indicating that other processes than surface turbulent transfer are important for hurricane intensity.

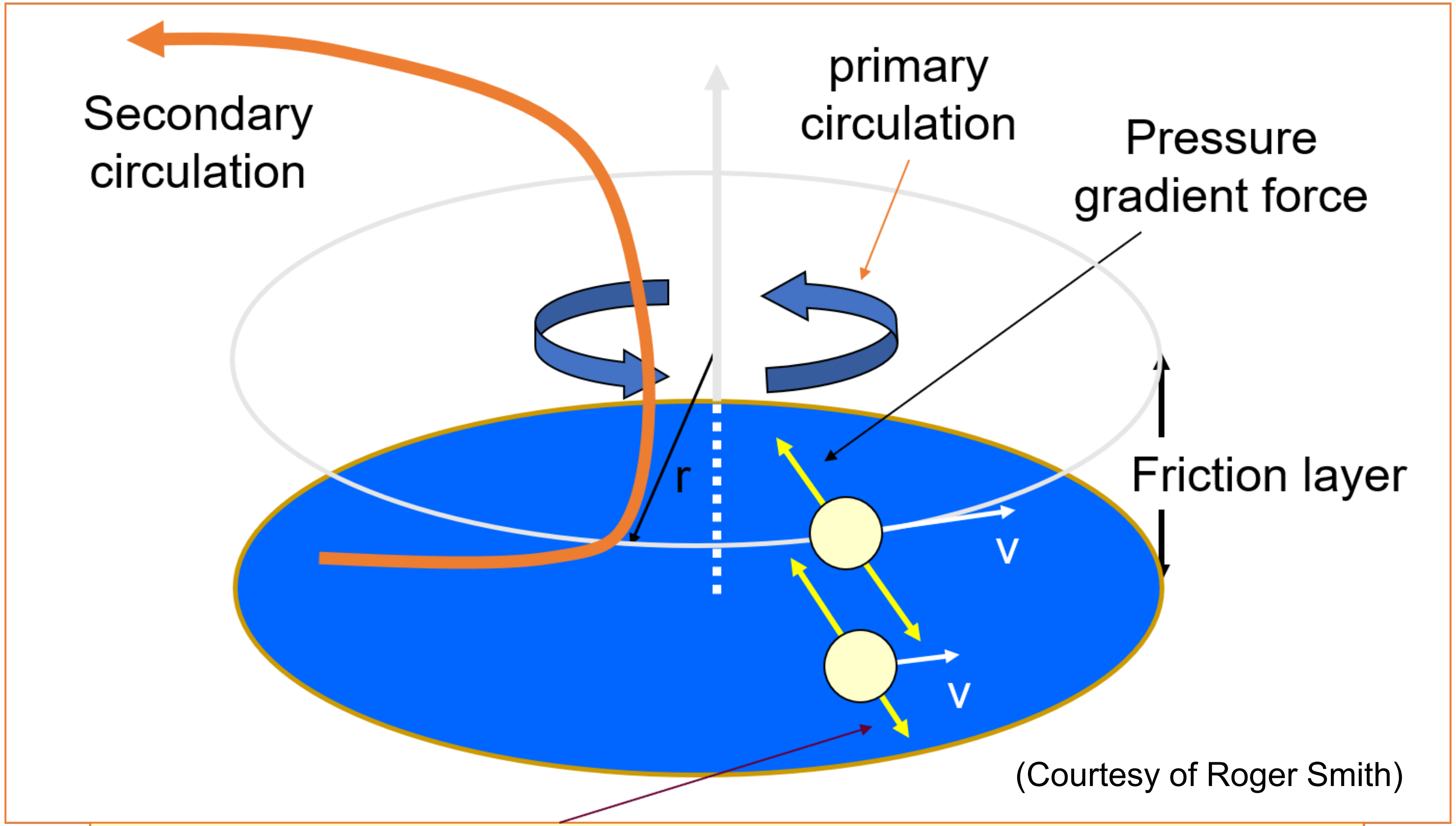

Centrifugal force and Coriolis force are reduced by friction

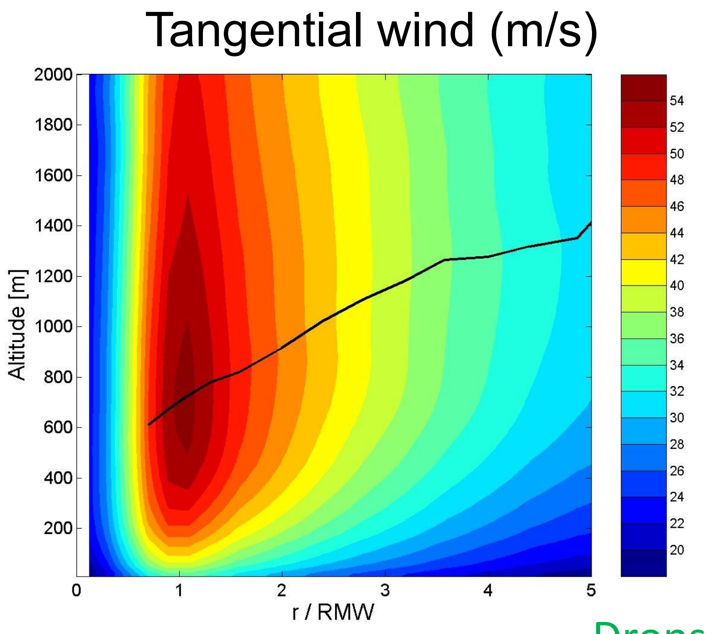

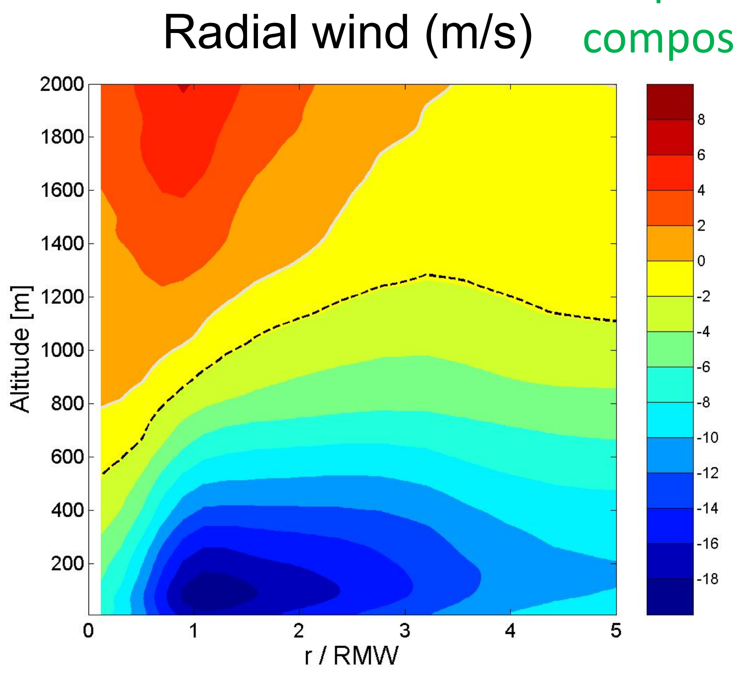

Dropsonde composites

Agradient force

$$\mathrm{AF} = -\frac{1}{\rho}\frac{\partial p}{\partial r} + \frac{v^2}{r} + fv$$

Boundary-layer height scales in hurricanes based on dropsonde composites

(Zhang et al. 2011)

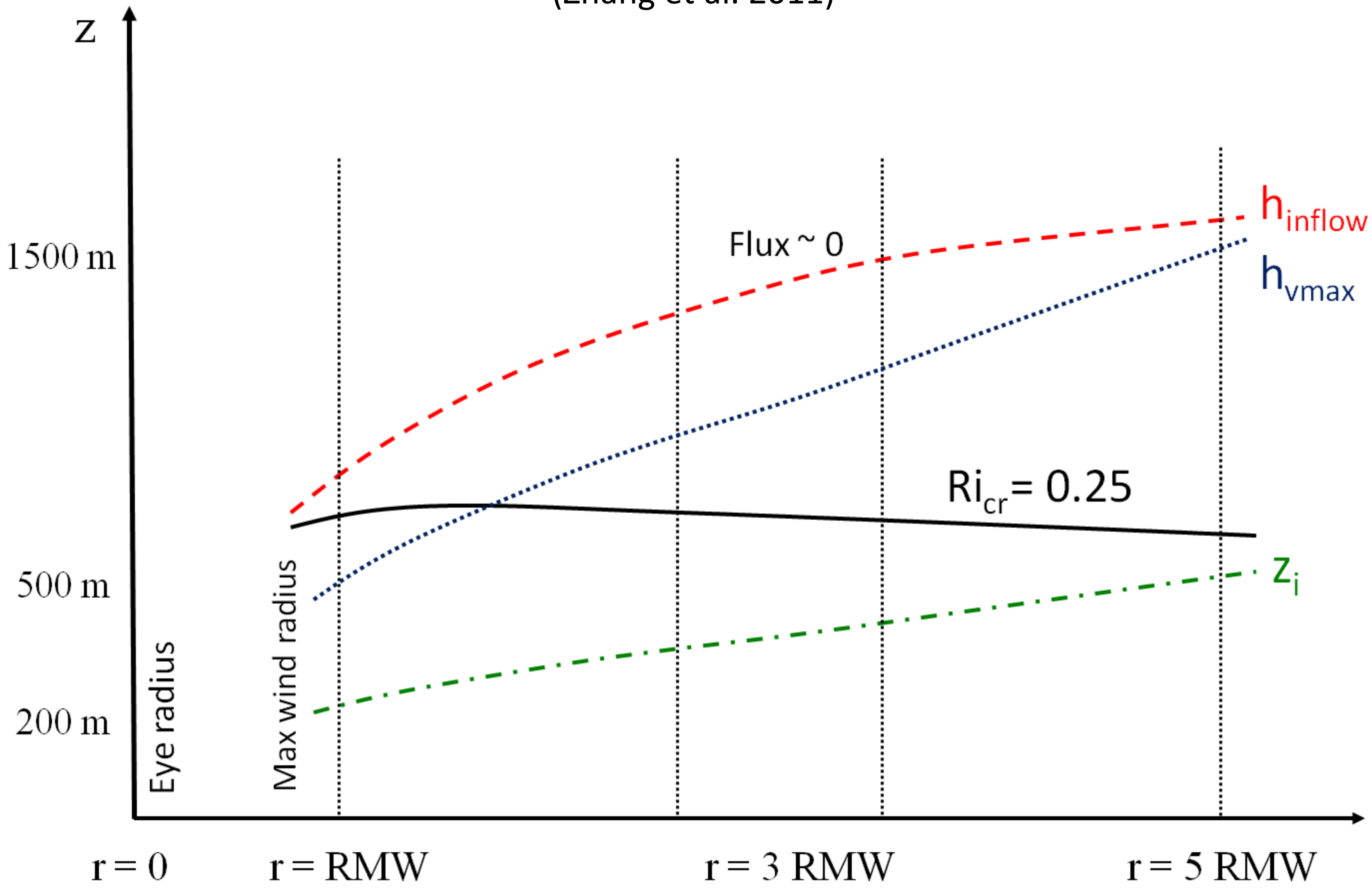

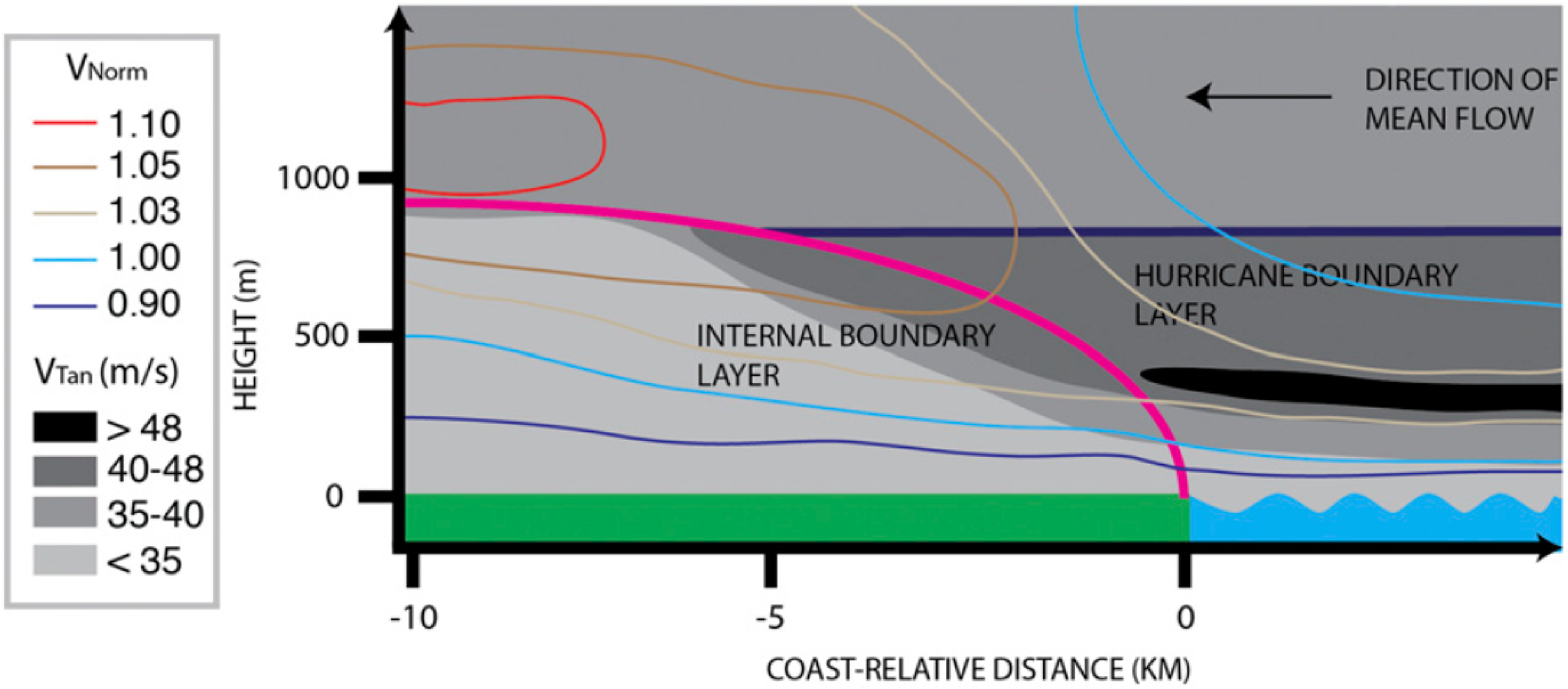

FIG. 14. Conceptual model of the HBL transition across the coastal interface for Hurricane Irene. The dark blue line represents the height of the pre-existing HBL that results from HBL dynamics over the open ocean. The magenta curve represents the growth of the internal boundary layer response to the surface roughness discontinuity at the coast. The tangential wind V_{tan} is shown via the color-filled contours according to the legend. The line contours according to the legend indicate the approximate value of the mean state of the coast-relative normalized wind V_{Norm}. The mean flow is directed from right to left (toward the coast).

(Alford et al. 2020)

Sensitivity of Simulated Hurricane Intensity to PBL Physics

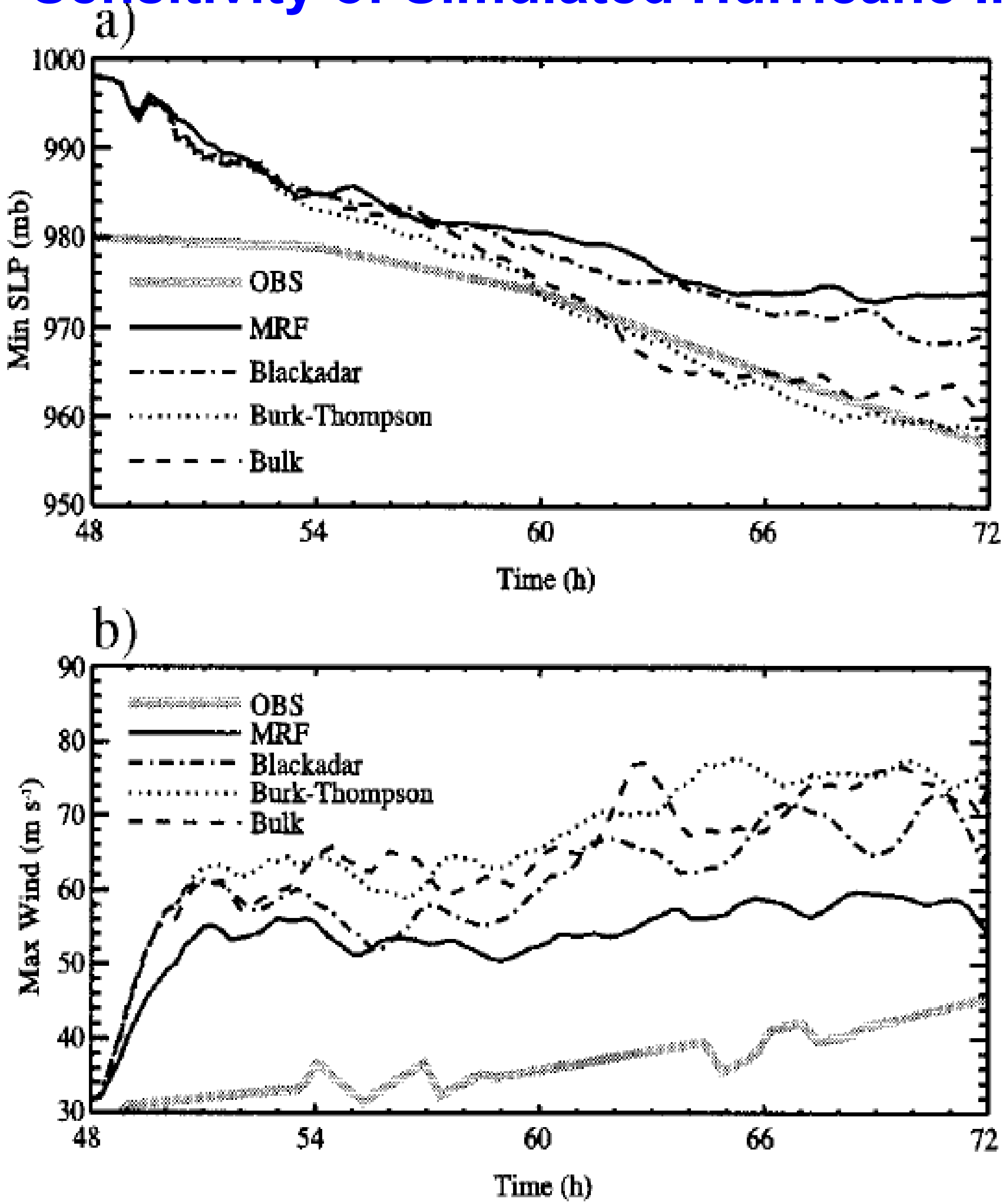

(Braun and Tao, 2000)

MM5 simulations of Hurricane Bob (1991)

➔ Skillful prediction of intensity change requires an accurate representation of the boundary layer.

Sensitivity of storm intensity to PBL schemes in idealized HWRF simulations

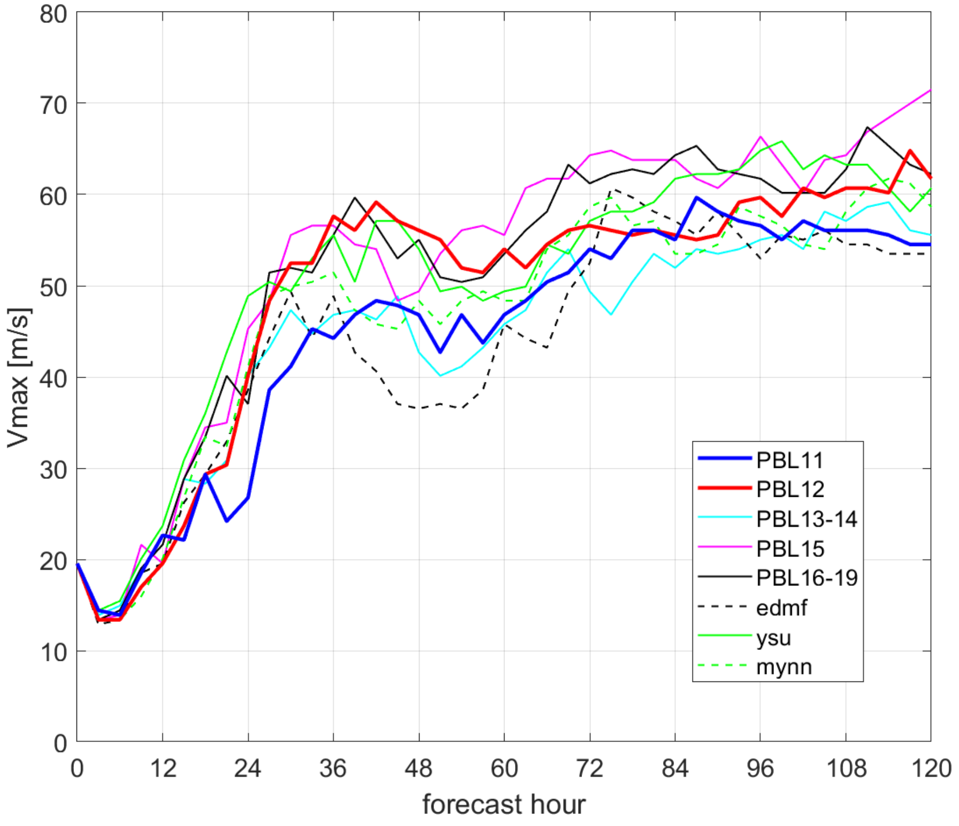

Table 1. Summary of the main differences in different versions of the planetary boundary layer (PBL) schemes in Hurricane Weather Research and Forecasting model (HWRF). GFS denotes Global Forecast System and EDMF denotes eddy diffusivity and mass flux. (Zhang et al. 2020)

HWRF Version	Year	PBL Scheme	Alpha Parameter	Critical Richardson Number	Referred to as
3.3a	2011	GFS	1.0	0.5	PBL11
3.4a	2012	GFS	0.5	0.25	PBL12
3.5a 3.6a	2013 2014	GFS	0.7	Varies with Rossby number	PBL13–14
3.7a	2015	GFS	Varies with wind speed	Varies with Rossby number	PBL15
3.8a 3.9a 4.0a	2016 2017 2018 2019	GFS EDMF	Varies with wind speed and height	Varies with Rossby number	PBL16–19

Eddy diffusivity $$K_m = k\,(u_*/S)\,z\,\{\alpha\,(1 - z/h)^{2}\}$$

Impact of vertical turbulent mixing on hurricane forecasts

(Zhang et al. 2015)

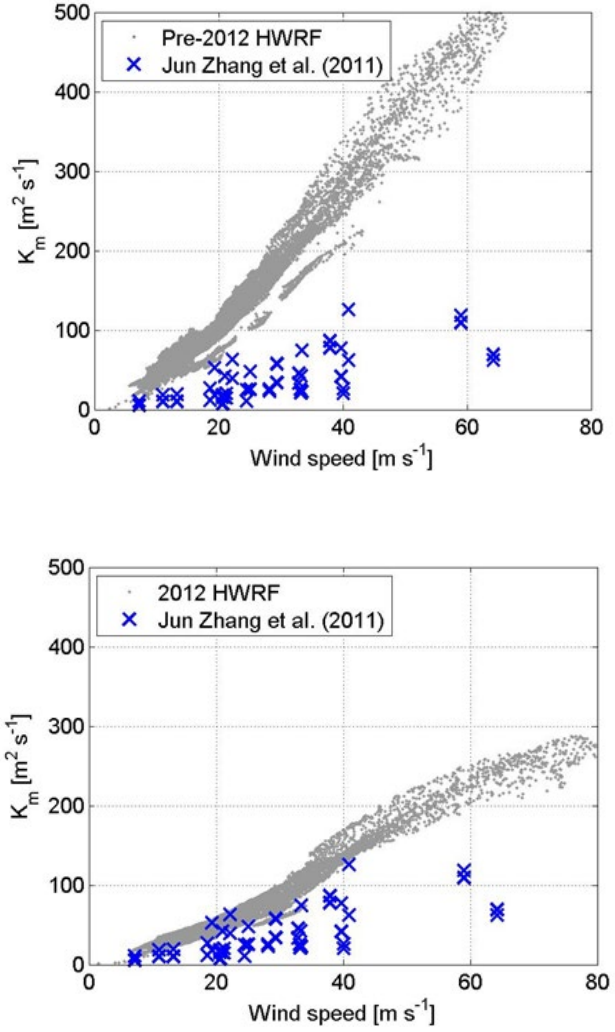

$$K_m = k\,(u_*/S)\,z\,\{\alpha\,(1 - z/h)^2\}$$

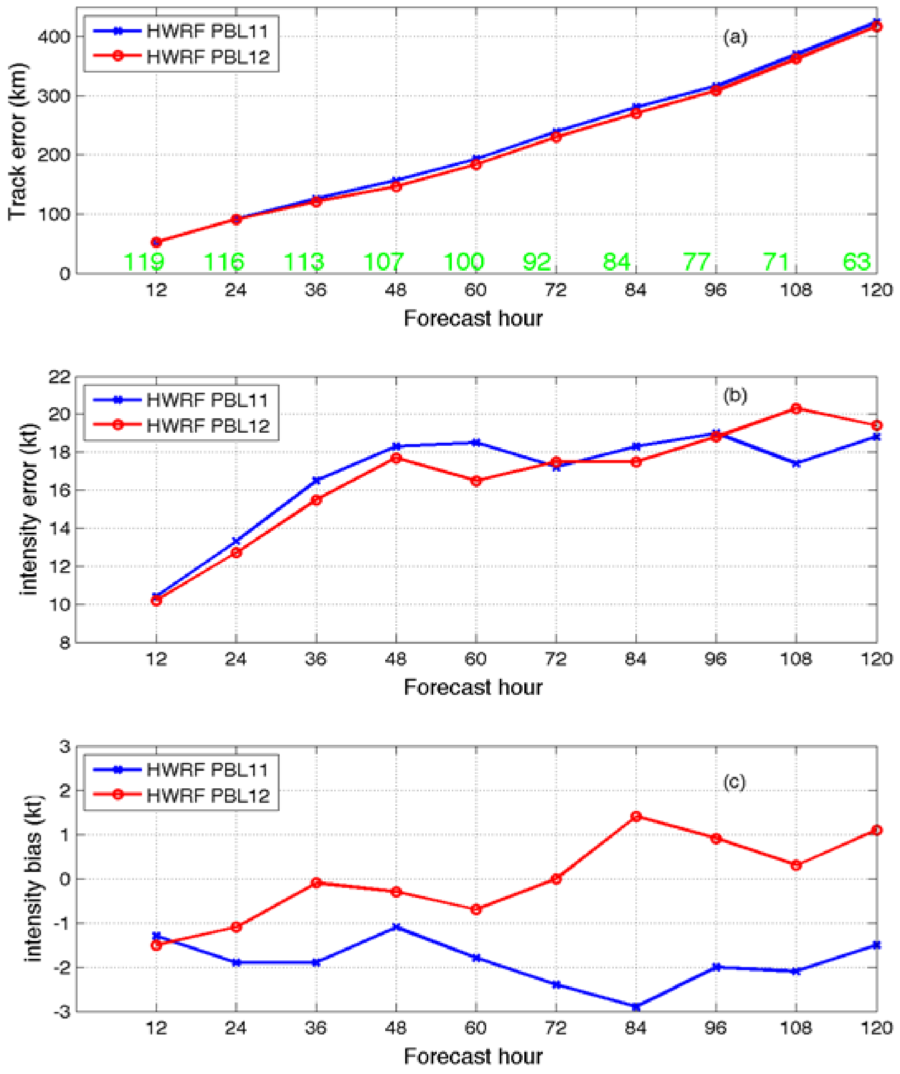

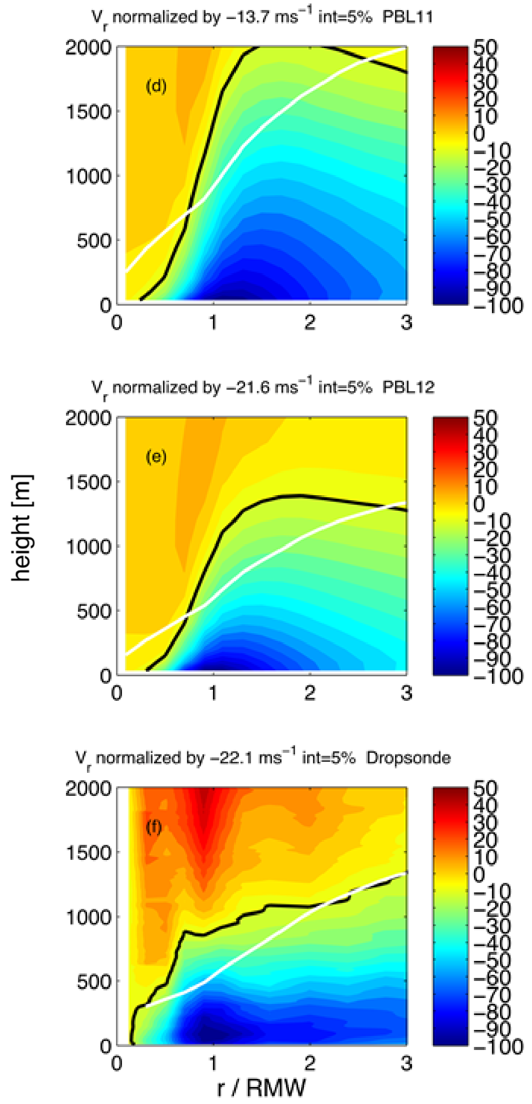

PBL11

Incorrect Km

Obs-corr Km

PBL12

Dropsonde Composite

observation

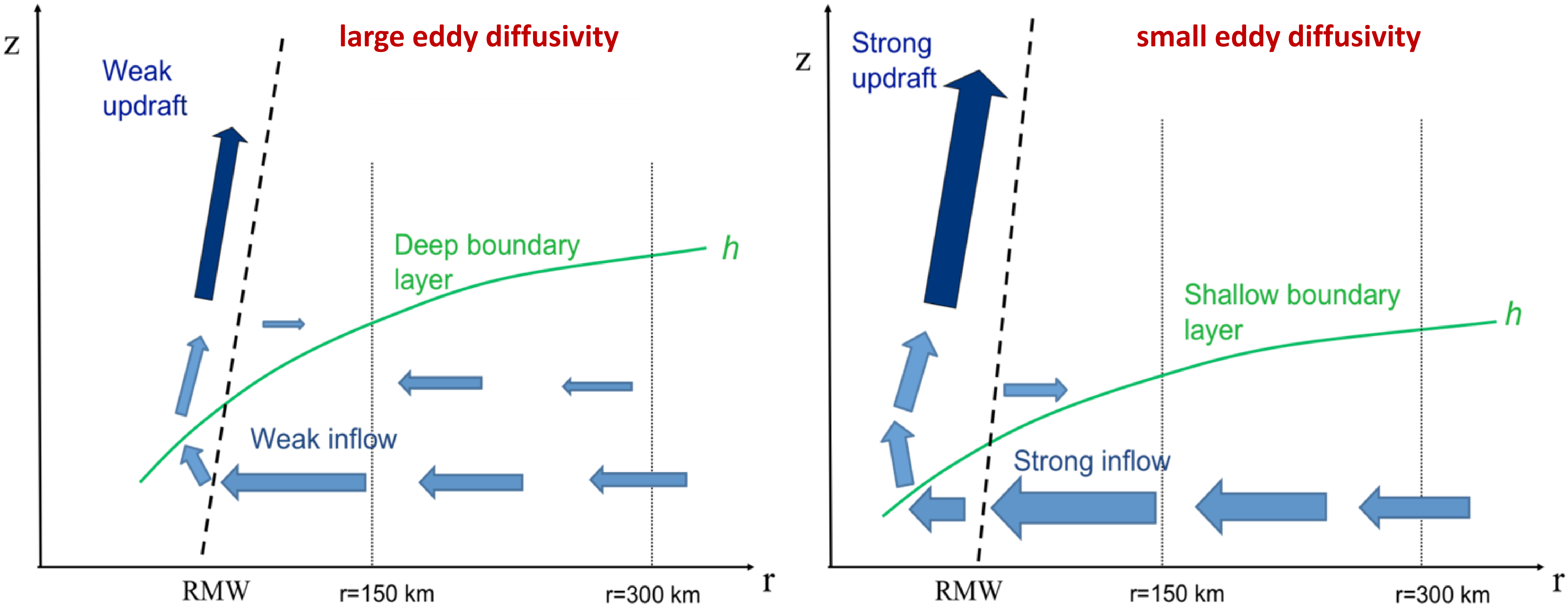

- The radial inflow is stronger for the case with smaller vertical diffusion in the boundary layer.
- As this radial inflow travels past the radius of maximum wind (RMW), its greater inertia will carry it further inward, leading to a stronger azimuthal wind maximum in the boundary layer.
- Furthermore, the base of the eyewall updraft will be at smaller radius, which further favors intensity due to the greater inertial stability there.

Hurricane intensification and Boundary layer recovery

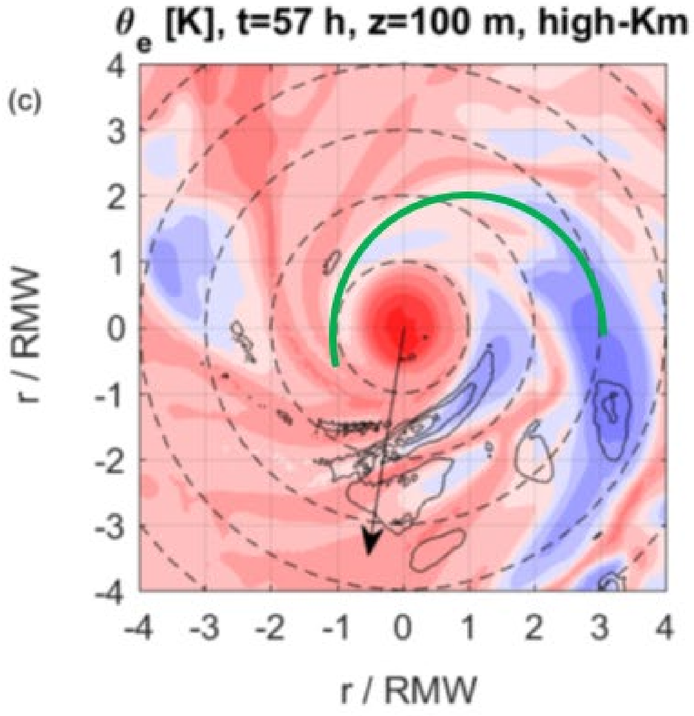

Green curve shows inflow trajectory

Black arrow shows the environmental shear direction

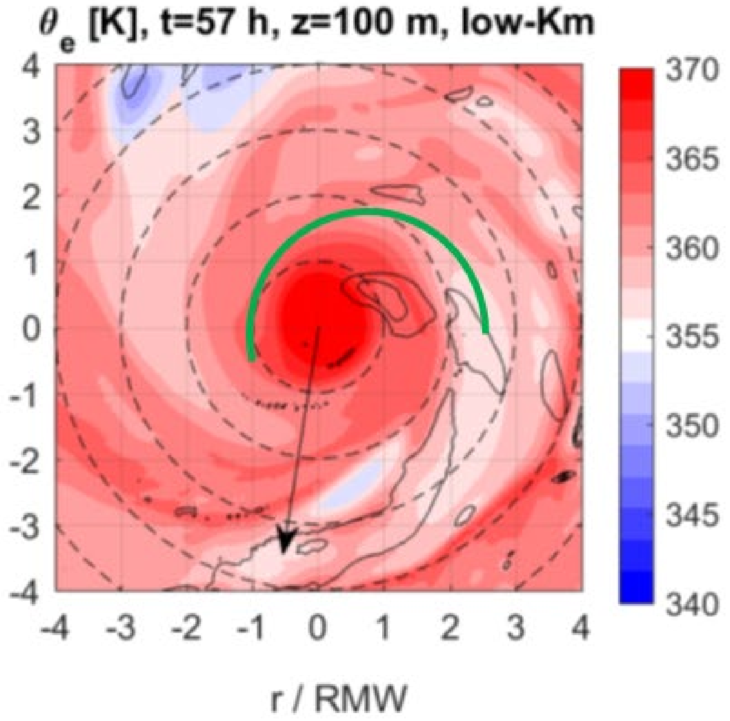

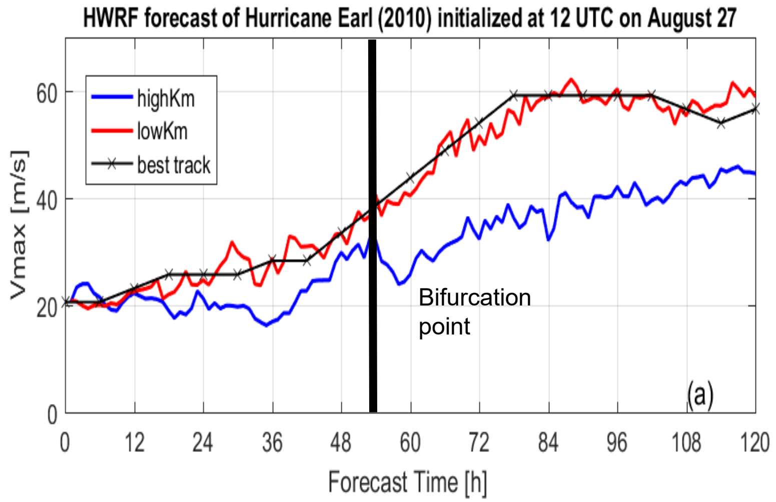

- ➢ The entropy (depicted by ϴe) in the boundary layer is lower in the high-Km forecast than in the low-Km forecast before the onset of rapid intensification.
- ➢ Surface enthalpy fluxes are enough to recover the low-entropy air from the upshear-left quadrant to the downshear-right quadrant in the low-Km forecast, but they are not enough for boundary layer recovery in the high-Km forecast.

(Zhang and Rogers 2019)

Impacts of horizontal turbulent mixing on Hurricane Forecasts

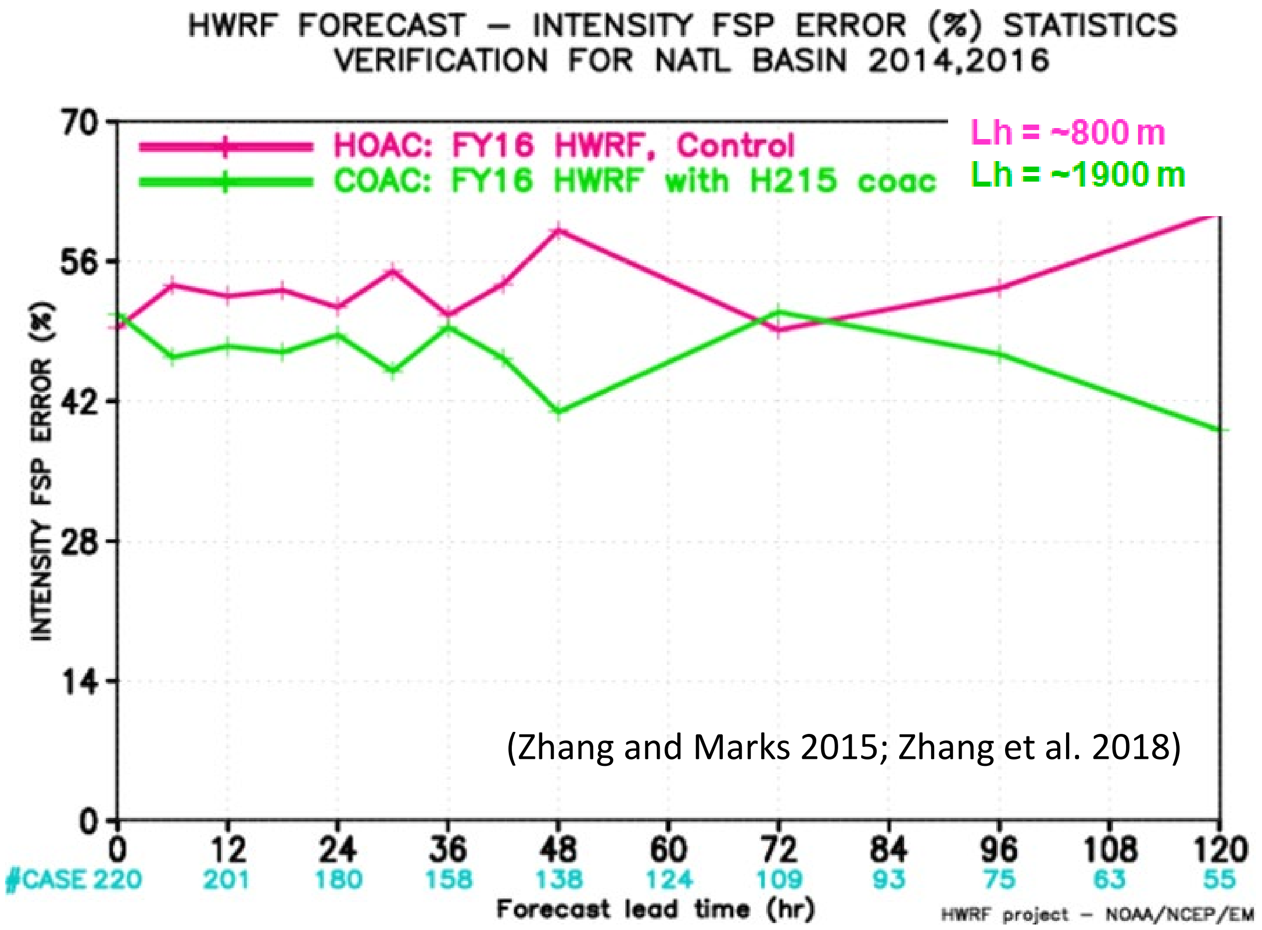

(Zhang and Marks 2015; Zhang et al. 2018)

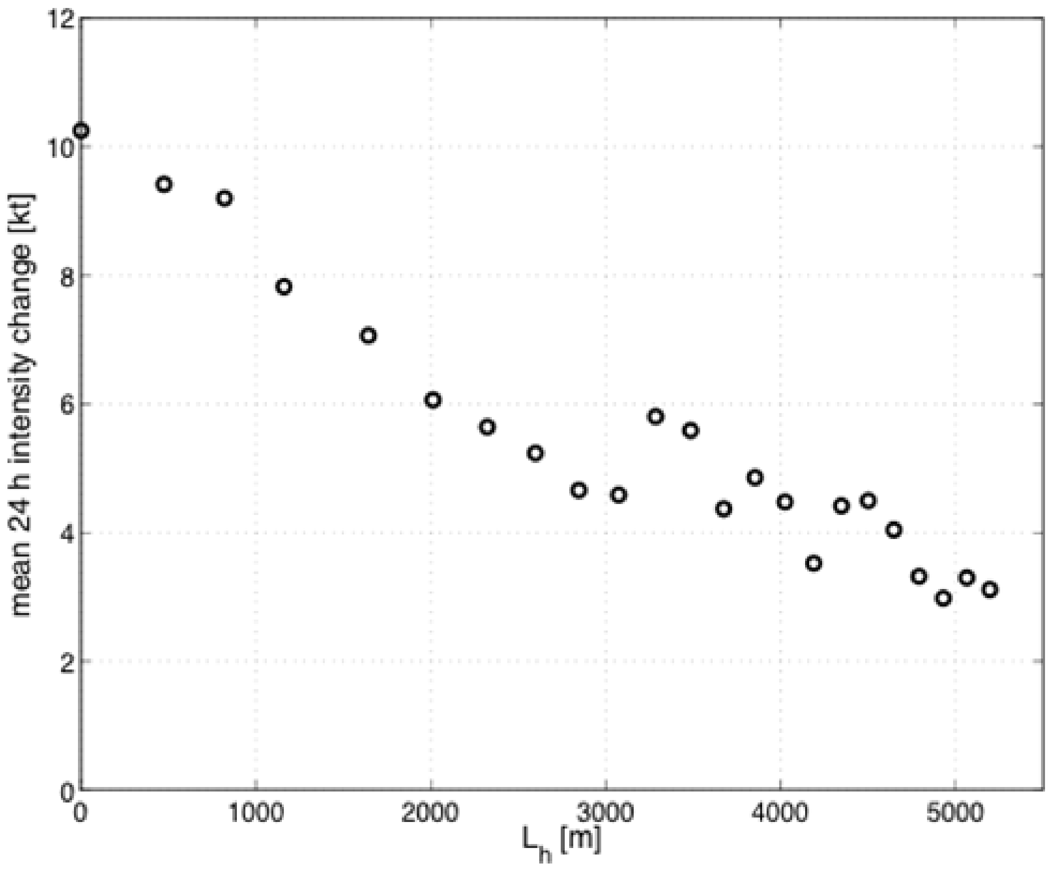

- ➢ The horizontal mixing length (Lh) was reduced in H216 to be close to observational estimates given by Zhang and Montgomery (2012).

Challenges and Gaps

1. Direct observations of turbulent fluxes in the boundary layer of the eyewall region
2. Collocated observations of flux, wave, current and sea spray in the hurricane-force wind regime
3. In-situ observations of the hurricane boundary-layer rolls
4. Continuous observations of the boundary-layer structure before and during hurricane rapid intensification
5. Observations of the boundary-layer thermodynamic structure in hurricanes over land
6. Definition of the hurricane boundary layer height
7. Effects of entrainment on hurricane intensity change
8. Effects of scale-aware PBL schemes on hurricane intensity in the gray zone
9. Effects of boundary-layer processes on hurricane intensity during landfalls
10. Effects of dissipative heating on hurricane intensity
11. Diurnal variation of the hurricane boundary-layer structure

Near-term possibilities

- Conduct Hurricane Ocean Survey and Boundary Layer Experiments with advanced technologies (Saildrones, Gliders, Uncrewed aircraft, IRsondes,etc.) to collect more observations at the air-sea interface

https://www.aoml.noaa.gov/wp-content/uploads/2021/04/2021HFP_EarlyStage_Science_HBL.pdf

https://www.aoml.noaa.gov/wp-content/uploads/2021/04/2021HFP_OceanSurvey_Science.pdf

https://www.aoml.noaa.gov/wp-content/uploads/2021/04/2021HFP_MatureStage_Science_RICO_SUAVE.pdf

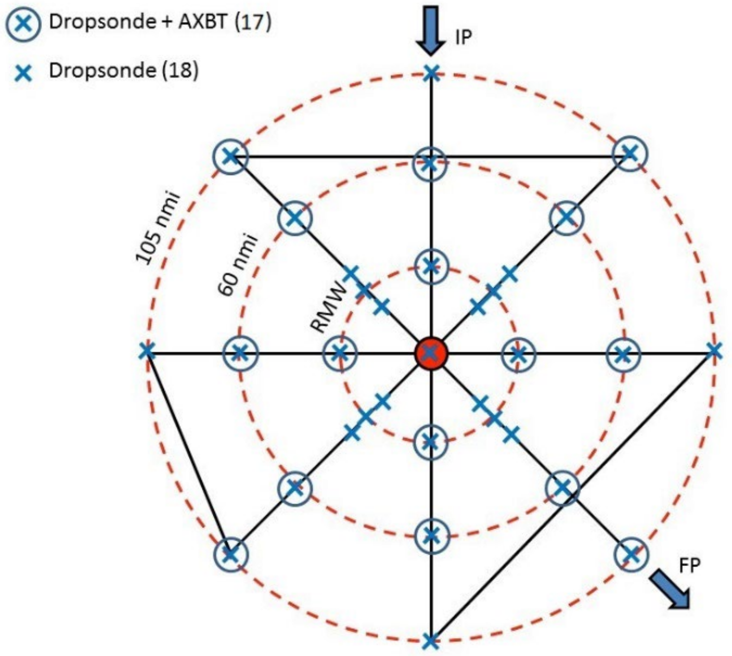

(Zhang et al. 2017)

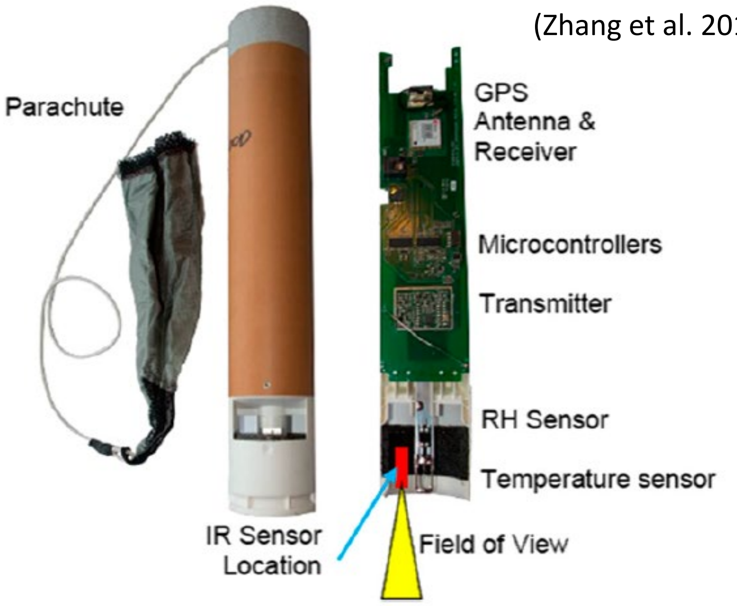

FIG. 1. A schematic of the (left) IRsonde appearance and (right) inside view of the sensors of the IRsonde.

(Cione et al. 2020)

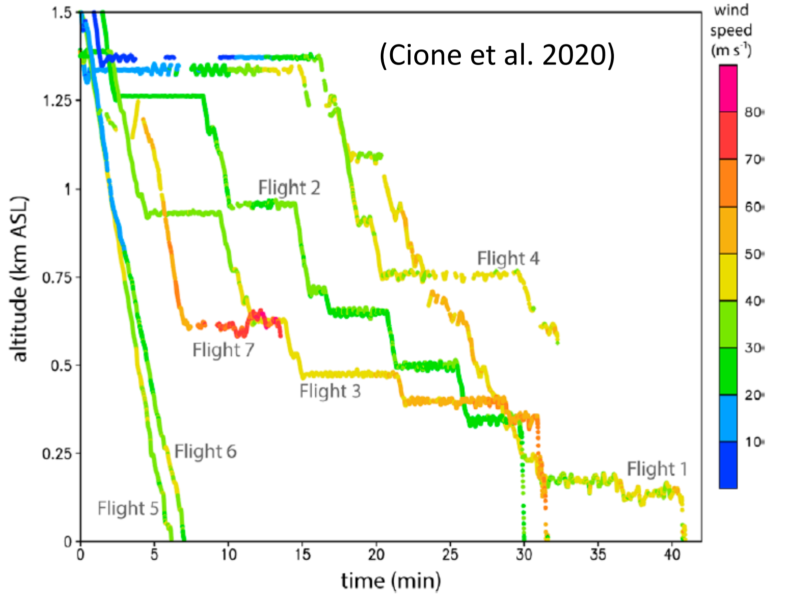

Fig. 6. Summary of all wind speed data collected during Coyote sUAS flights in 2017–18 (colored dots, m s^{-1}) as a function of time and height above sea level (ASL). Flights 1–4 and 7 were typical "stepped descent" flight patterns, while flights 5–6 were "glider" flights.

Near-term possibilities

- Use Large Eddy Simulation (LES) data for model evaluation in the absence of or as a complement to turbulence observations

Note that this method still requires observations to assess the validity of the LES.

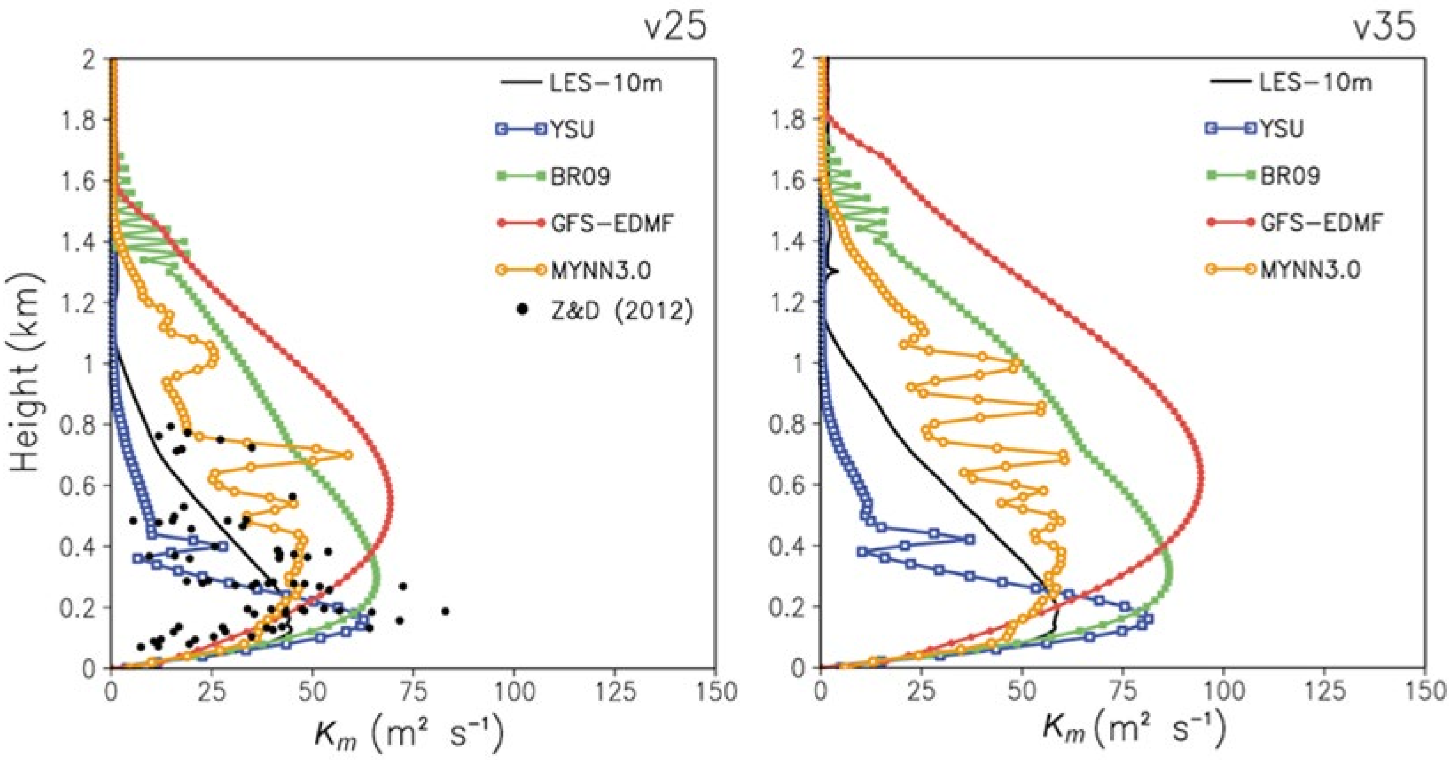

(Chen et al. 2021 in review; Zhang and Drennan 2012)